FORMATION CONTROL OF SATELLITES SUBJECT TO J2 PERTURBATIONS

1. INTRODUCTION

Formation flying of spacecraft is a key enabling technology for future complex missions in distributed sensing using a group of cluster of small satellites. The main benefits include graceful degradation during satellite failure, improved flexibility by reconfiguring to perform different tasks and open new mission possibilities that would not be possible with a single monolithic satellite. Examples include the US Air Force TechSat-21 for virtual satellite concept, Laser Interferometer Space Antenna (LISA) mission to detect gravity waves, Gravity Recovery and Climate Experiment (GRACE), TanDEM-X, PRISMA and Hawkeye 360 for signal detection and localization. One of the main challenges of satellite formation flying is the guidance, navigation and control design solution to achieve the formation objectives.

The problem of satellite formation control design has been extensively studied. The Hill-Clohessy-Wiltshire (HCW) linearized equations [1-3] are commonly used to describe the relative motion of two satellites in circular orbits without orbital perturbations, as these are constant coefficient differential equations with simple analytical solutions with in-track secular drift term which can be removed by proper initialization. Moreover, these analytical solutions enable intuitive design of satellite formations. The inherent limitations of the linear time-invariant (LTI) HCW model is that it ignores the secular effects of the dominant J_2 perturbation ,due to the oblateness of the Earth, which introduces a secular drift in satellite orbit. To mitigate this limitation, Schweighart and Sedwick [4] modified the HCW equations to include the J_2 perturbation on a circular reference orbit. However, assuming circular reference orbit will result in considerable errors when the eccentricity of the reference orbit increases. Lawden [5] first presented a solution with singularities for the relative motion of two spacecraft in unperturbed eccentric orbits and Tschauner and Hempel [6] also presented a similar set of equations that also use true anomaly as the independent variable. Carter [7] later provided a set of solutions without singularities. Lane and Axelrad [8] developed a time-explicit linearized closed-form solution for bounded relative elliptical orbits but expressed in curvilinear radial, in-track, cross-track (RIC) frame. In particular, Inalhan et al [9] have extended the LTI HCW model to a linear-parameter-varying (LPV) model for unperturbed elliptical orbit. However, in view of the growing vision for tighter space formation in perturbed elliptic orbit, there is a drive to derive higher fidelity non-linear model for eccentric orbits which is tractable for controller design. An alternative formulation is to parameterize the relations satellite motion using classical orbital elements instead of the Cartesian co-ordinates. Orbital perturbations will cause the orbital parameters to drift away from desired parameters and this will result in orbit element differences. The merit of this approach in a control perspective is that the satellites are maintained in their natural orbits instead of keeping the formation fixed in a Cartesian frame. Koenig et al. [9] modelled the satellite relative motion in perturbed eccentric orbits using a mean relative orbital element (ROE) state representation. In the presence of J_2 perturbation, the osculating elements will experience both short-period oscillations and secular shift. The mean orbital elements captures the secular drift and thus the J_2-perturbed osculating elements can be approximated by adding the mean orbital elements to the time-varying short-period variation of each element caused by J_2. The latter short period variations can be calculated as a function of the osculating orbit elements [10]. In view of the above discussion, this report investigates

both the use of the simpler linearized HCW relative motion model for in-plane/along track formation controller synthesis and the non-linear perturbed eccentric model based on the mean ROE which is more amenable for cross-track oscillation formation controller design. These models contain inherent inaccuracies and are only adopted for the design of the different formation controllers. Owing to these limitations, the more accurate perturbed eccentric model will be used to determine the requisite initial conditions as the desired set-points to maintain a stable formation. The long term prediction of the formation trajectories will be separately propagated on the ground using higher fidelity software, e.g. STK, to determine the predicted satellite states for the next control update iteration cycle.

The first part of the formation control problem is to determine a formation geometry that meets the mission requirements. Owing to the influence of various perturbations in the space environment, formation flying satellites will not be able to maintain specific configurations over extended operating durations. In order to meet the designed mission objectives, active satellite control is needed to maintain the formation configuration. The Linear Quadratic (LQ) optimal control theory is a mature and popular state space design method applicable for linear systems which regulates the desired output variables and minimize the control effort. A discrete-time LQ control law based on HCW equations was presented by Sparks [10] to overcome J_2 perturbations in orbit. However, control strategies for relative position control must also address practical constraints including limited constant thrust force and operational concerns such as control activation time constraints due to satellite power considerations.

In this report, we shall address the guidance and control design techniques for formation initialization and maintenance. Typical tight formation flying requires precise position requirements and hence will require much more stringent control. Hence, most published literature, either explicitly propose or implicitly assume a decentralized approach to achieve satellite autonomy and reduce the need for ground support. However, this approach necessitates the formation flying satellites to communicate among themselves via inter-satellite link to distribute their respective satellite states, position and velocity, to enable real-time autonomous decision making. This will incur cost penalty to implement the inter-satellite communications and on-board processing as well as add mission complexity to co-ordinate and perform relative pointing to distribute individual satellite state information to the rest of the satellites in the formation.

In contrast to the above closed loop autonomous precise control for close formation, we focus on a ground-based centralized solution for formation flying. F

or coarse satellite positioning requirements similar to what we envisaged for our missions, this can be more effectively achieved through open loop behaviour with occasional corrections from the ground. We adopt an open-lop control strategy which simplifies the implementation and provides a cost effective solution to meet the ‘loose’ formation control requirements of several tens of kilometres baseline separation. Our solution will entail the individual satellites to transmit their respective states to the ground station which will process and compute the appropriate control commands for each of the satellite. These computed commands will subsequently be uplinked to the respective satellites and activated on-board at assigned time and for specific duration.

This report is organised as follows: Section 2 reviews and analyses the existing models on relative motion dynamic models and the control solution for formation initialization and

maintenance is presented in Section 3. The guidance strategy and the ground-based implementation control is discussed in Section 4 and simulation results obtained from MatLab and high fidelity STK software are detailed in Section 5. Finally, the conclusion is formulated in Section 6.

2. RELATIVE MOTION DYNAMICS MODEL

2.1 Cartesian Coordinate Frames

The two different co-ordinate reference frames adopted in this report are depicted in Fig. 1 and defined in the following subsections.

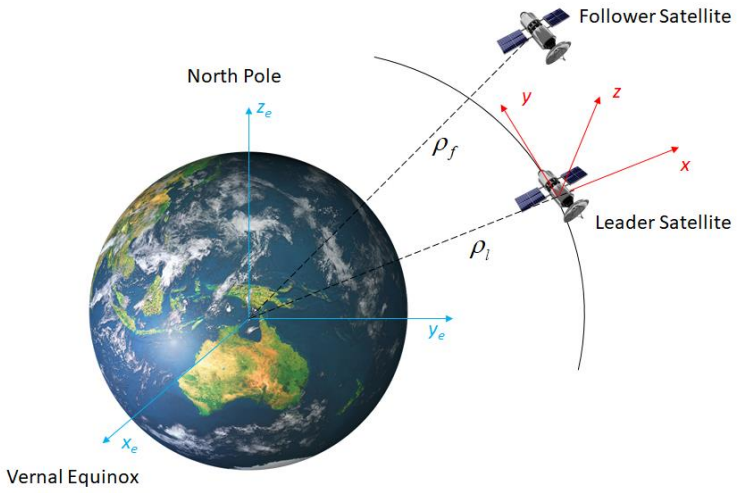

Fig. 1 Cartesian Co-Ordinate Frames

2.1.1 *Earth-Centred Inertial (ECI) Frame*

The motion of the satellites orbiting the Earth is described in the Earth Centered Inertial (ECI) frame. In this frame, the centre of the Earth is the origin. The z_e–axis is directed along the rotation axis of the Earth towards the celestial north pole, the x_e-axis is directed towards the vernal equinox and the -axis completes the right-handed orthogonal frame. Here, r_l represents a radial vector from the Earth's centre of mass to the leader satellite in ECI frame.

2.1.2 *Euler-Hill Frame*

The relative motion of two satellites orbiting the Earth is described in the Local Vertical Local Horizontal (LVLH) co-ordinate system, also known as the Euler-Hill frame, with its origin located in the mass centre of the leader satellite. The x-axis in this LVLH co-ordinate system,

is in the direction of the vector pointing from the centre of the Earth to the leader satellite, and the z-axis points in the orbit normal direction. The y-axis completes the right-handed orthogonal frame. The basis vectors of the Hill frame can be expressed as:

$$\hat{x} = \frac{r_l}{\|r_l\|},\ \hat{z} = \frac{h}{|h|},\ \hat{y} = \hat{z} \times \hat{x}, \tag{2.1}$$

where $h = r_l \times \dot{r}_l$ is the angular momentum vector of the orbit.

2.2 Equations of Relative Motion

The dynamic model of the leader satellite in a reference orbit in ECI frame can be obtained according to Kepler's equation:

$$\begin{aligned} &m_l \ddot{r}_l + m_l \left(M + m_l\right) \frac{G}{\|r_l\|^3} r_l + D_l = u_l \\ &m_l \ddot{r}_l + m_l \frac{\mu}{\|r_l\|^3} r_l + D_l = u_l \end{aligned} \tag{2.2}$$

$$\|r_l\| = \frac{a_l \left(1 - e_l^2\right)}{\left(1 + e_l \cos f_l\right)} \tag{2.3}$$

where $\mu = G\,M$ is the gravitational constant, m_l is the mass of the leader satellite, $M \gg m_l$ as the Earth's mass, $D_l \in \mathbb{R}^3$ is the disturbance force acting on the leader satellite such as external perturbation due to J_2 zonal harmonics effect, solar radiation pressure, drag, $u_l \in \mathbb{R}^3$ is the control force generated by the leader satellite and a_l, e_l, f_l are the leader's orbit semi-major axis, eccentricity and true anomaly, respectively. Similarly, the inertial equations of motion of the follower are given by

$$\begin{aligned} &m_f \ddot{r}_f + m_f \left(M + m_f\right) \frac{G}{\|r_f\|^3} r_f + D_f = u_f \\ &m_f \ddot{r}_f + m_f \frac{\mu}{\|r_f\|^3} r_f + D_f = u_f \end{aligned} \tag{2.4}$$

$$\|r_f\| = \frac{a_f \left(1 - e_f^2\right)}{\left(1 + e_f \cos f_f\right)} \tag{2.5}$$

where r_f represents a radial vector from the Earth's centre of mass to the satellite in ECI frame, m_f is the mass of the follower satellite, $M \gg m_f$ as the Earth's mass, $D_f \in \mathbb{R}^3$ is the disturbance force acting on the follower satellite, $u_f \in \mathbb{R}^3$ is the control force to the follower satellite and a_f, e_f, f_f are the follower's orbit semi-major axis, eccentricity and true anomaly,

respectively. Let ρ denotes the relative vector of follower satellite to the leader satellite in ECI frame. Hence,

$$p = r_f - r_l \tag{2.6}$$

and

$$m_f \ddot{\rho} + m_f \mu \left(\frac{(r_l + \rho)}{\|r_l + \rho\|^3} - \frac{r_l}{\|r_l\|^3} \right) + \frac{m_f}{m_l} U_l + D_f - \frac{m_f}{m_l} D_l = U_f \tag{2.7}$$

Assuming that $m_l = m_f = m$, we obtain

$$m\ddot{\rho} + m\mu \left(\frac{(r_l + \rho)}{\|r_l + \rho\|^3} - \frac{r_l}{\|r_l\|^3} \right) = D + U \tag{2.8}$$

where $D = D_l - D_f$, $U = U_f - U_l$ are the differential perturbation forces and control forces respectively.

In the LVLH frame, the relative acceleration vector $\ddot{\rho}$ in LVLH frame is given by

$$\ddot{\rho} = \begin{bmatrix} \ddot{x} - 2\dot{\theta}_l \dot{y} - \ddot{\theta}_l y - \dot{\theta}_l^2 x & \ddot{y} + 2\dot{\theta}\dot{x} + \ddot{\theta}_l x - \dot{\theta}^2 y & \ddot{z} \end{bmatrix}^T \tag{2.9}$$

since

$$\ddot{\rho} = \frac{d^2}{dt^2} \begin{bmatrix} x \\ y \\ z \end{bmatrix} + 2 \times \begin{bmatrix} 0 \\ 0 \\ \dot{\theta}_l \end{bmatrix} \times \frac{d}{dt} \begin{bmatrix} x \\ y \\ z \end{bmatrix} + \frac{d}{dt} \begin{bmatrix} 0 \\ 0 \\ \dot{\theta}_l \end{bmatrix} \times \begin{bmatrix} x \\ y \\ z \end{bmatrix} + \begin{bmatrix} 0 \\ 0 \\ \dot{\theta}_l \end{bmatrix} \times \begin{bmatrix} 0 \\ 0 \\ \dot{\theta}_l \end{bmatrix} \times \begin{bmatrix} x \\ y \\ z \end{bmatrix} \tag{2.10}$$

where $\dot{\theta}_l$ is the angular rate of the rotating Euler-Hill frame relative to the inertial ECI frame. Denote $q = \begin{bmatrix} x & y & z \end{bmatrix}^T$ as the relative position vector in the LVLH frame, then Eqn. (2.8) can be arranged into the following form [13]:

$$\ddot{q} + C\left(\dot{\theta}_l\right)\dot{q} + F\left(\dot{\theta}_l, \ddot{\theta}_l\right) q + n\left(q, \|r_l\|\right) = \frac{D}{m} + \frac{U}{m} = d + u \tag{2.11}$$

where

$$C\left(\dot{\theta}_l\right) = \begin{bmatrix} 0 & -2\dot{\theta}_l & 0 \\ 2\dot{\theta}_l & 0 & 0 \\ 0 & 0 & 0 \end{bmatrix}, F\left(\dot{\theta}_l, \ddot{\theta}_l\right) = \begin{bmatrix} -\dot{\theta}_l^2 & -\ddot{\theta}_l & 0 \\ \ddot{\theta}_l & \dot{\theta}_l^2 & 0 \\ 0 & 0 & 0 \end{bmatrix}, n\left(q, \|r_l\|\right) = \begin{bmatrix} \dfrac{\mu\left(\|r_l\| + x\right)}{\|R + q\|^3} - \dfrac{\mu}{\|r_l\|^2} \\ \dfrac{\mu y}{\|R + q\|^3} \\ \dfrac{\mu z}{\|R + q\|^3} \end{bmatrix} \tag{2.12}$$

and $R = \begin{bmatrix} \|r_l\| & 0 & 0 \end{bmatrix}^T$, d and u are the differential acceleration perturbations and control acceleration respectively.

2.2.1 *Unperturbed Elliptical Reference Orbit in Euler-Hill Frame*

The relative motion dynamics (2.12) for an eccentric reference orbit can also be expressed in terms of its individual components in the following *nonlinear* differential equations [14]:

$$\begin{aligned}
\ddot{x} - 2\dot{\theta}_l \dot{y} - \dot{\theta}_l^2 x - \ddot{\theta}_l y &= -\frac{\mu\left(\|r_l\| + x\right)}{\left[\left(\|r_l\| + x\right)^2 + y^2 + z^2\right]^{3/2}} + \frac{\mu}{\|r_l\|^2} + d_x + u_x \\
\ddot{y} + 2\dot{\theta}_l \dot{x} + \dot{\theta}_l^2 y + \ddot{\theta}_l x &= -\frac{\mu y}{\left[\left(\|r_l\| + x\right)^2 + y^2 + z^2\right]^{3/2}} + d_y + u_y \\
\ddot{z} &= -\frac{\mu z}{\left[\left(\|r_l\| + x\right)^2 + y^2 + z^2\right]^{3/2}} + d_z + u_z
\end{aligned} \tag{2.13}$$

where $\begin{bmatrix} d_x & d_y & d_z \end{bmatrix}^T$ and $\begin{bmatrix} u_x & u_y & u_z \end{bmatrix}^T$ are, respectively, the components of external differential acceleration perturbations and differential control accelerations represented in the Euler-Hill frame.

2.2.2 *Unperturbed Circular Reference Orbit*

In Section 2.2.1, equation (2.10) describes the general nonlinear equations of relative motion for arbitrary reference orbits of the leader satellite. A simpler form of the relative motion equations is obtained if the leader satellite lies in a circular orbit. For a circular reference orbit, $\|r_l\| = a$ is the radius of the circular orbit and $\dot{\theta}_l = n = \sqrt{\mu / a^3}$ is the constant mean motion or equivalently the angular frequency of the leader satellite. Substituting into Equation (2.13), we have

$$\begin{aligned}
\ddot{x} - 2n\dot{y} - n^2 x &= -\frac{\mu\left(a + x\right)}{\left[\left(a + x\right)^2 + y^2 + z^2\right]^{3/2}} + \frac{\mu}{a_l^2} + d_x + u_x \\
\ddot{y} + 2n\dot{x} - n^2 y &= -\frac{\mu y}{\left[\left(a + x\right)^2 + y^2 + z^2\right]^{3/2}} + d_y + u_y \\
\ddot{z} &= -\frac{\mu z}{\left[\left(a + x\right)^2 + y^2 + z^2\right]^{3/2}} + d_z + u_z
\end{aligned} \tag{2.14}$$

Note that the nonlinear term in the denominator in the right hand side of Eqn. (2.14) can be simplified to

$$\begin{aligned}\left[(a+x)^2+y^2+z^2\right]^{-3/2} &= \left[a^2+2ax+x^2+y^2+z^2\right]^{-3/2} \\ &= \frac{1}{a^3}\left[1+\frac{2x}{a}+\frac{x^2+y^2+z^2}{a^2}\right]^{-3/2} \\ &\approx \frac{1}{a^3}\left(1-\frac{3x}{a}\right)\end{aligned} \tag{2.15}$$

Linearizing Eqn. (2.14) about the origin of the Euler-Hill frame, we have

$$\frac{\mu(a+x)}{\left[(a+x)^2+y^2+z^2\right]^{3/2}} \approx \frac{\mu}{a^3}(a+x)\left(1-\frac{3x}{a}\right) \approx n^2(a-2x)$$

$$\frac{\mu y}{\left[(a+x)^2+y^2+z^2\right]^{3/2}} \approx \frac{\mu y}{a^3}\left(1-\frac{3x}{a}\right) \approx n^2 y$$

$$\frac{\mu z}{\left[(a+x)^2+y^2+z^2\right]^{3/2}} \approx \frac{\mu z}{a^3}\left(1-\frac{3x}{a}\right) \approx n^2 z$$

which is the so-called HCW equations of motion [1,2]. The HCW describe the relative motion of a follower with respect to a leader satellite on a reference circular orbit in a set of linear differential equations. They are given in LVLH fame as follows:

$$\begin{aligned}\ddot{x} - 2n\dot{y} - 3n^2 x &= u_x \\ \ddot{y} \qquad\quad +2n\dot{x} &= u_y \\ \ddot{z} \qquad\quad +n^2 z &= u_z\end{aligned} \tag{2.16}$$

Note that 2 major assumptions are inherent in HCW equations:

1) The leader satellite is in a reference circular orbit.
2) Linearization of the differential gravitational acceleration if the distance between the reference and follower satellite, $\|\rho\|$ is small (few tens of kilometres) in comparison to their orbital radius a (refer to Eqn. (2.12)). (Note that these linearized equations are also applicable even if the follower's orbit is slightly elliptic and inclined with respect to the leader's reference orbit provided that the initial positions are small.)
3) It ignores the orbital perturbation forces $\begin{bmatrix} d_x & d_y & d_z \end{bmatrix}^T$.

2.2.3 *Unperturbed Elliptical Reference Orbit*

HCW equations have traditionally been used for rendezvous analysis, which typically involves relatively short time spans, and hence the assumptions made may not remain valid over an extended long period of time. The circular reference trajectory represents only an approximation of the actual perturbed relative satellite motion in the Hill frame. If the eccentricity of the leader's orbit is nonzero or if the separation between the two satellites increases (resulting in more significant J2 perturbation), then the following Lawden's [5]

equations with the true anomaly f_l as the independent variable or equivalently, Tschauner and Hempel (TH) [6] relative equations for elliptical satellite motion may be considered.

$$\begin{aligned} x'' &= \frac{3}{\kappa}x + 2y' \\ y'' &= -2x' \\ z'' &= -z' \end{aligned} \tag{2.17}$$

where $(\cdot)'$ and $(\cdot)''$ denote respectively the first and second derivative with respect to f_l and $\kappa = 1 + e_l \cos f_l$. By selecting appropriate integration constants it is possible to obtain periodic relation motion solutions [14] with higher-order harmonics due to the reference orbit eccentricity. It is apparent from the above equations that the relative satellite position is a function of the true anomaly and both of these values must be accurately computed. However, there is no easy and practical method to calculate the true anomaly, except for solving Kepler's equation which ignores orbital perturbation, which may result in instability for formation control design.

2.2.3 *Perturbed Circular Reference Orbit*

To overcome the inherent limitations of the HCW model, other formulations have been proposed to include the dominant J_2 perturbation, the second order zonal gravitational harmonics, which cause secular drifts on an orbit by rotating the line of apsides and precession of the line of nodes. In particular, Schweighart and Sedwick [4] modified the Hill's equations to obtain a high fidelity linearized relative motion of two satellites under the influence of the J_2 perturbation. The corresponding modified HCW equations are described below:

$$\begin{aligned} &\ddot{x} - 2nc\dot{y} - \left(5c^2 - 2\right)n^2 x = u_x \\ &\ddot{y} \quad + \quad 2nc\dot{x} \quad = u_y \\ &\ddot{z} \quad + \quad k^2 z \quad = 2lk\cos\left(kt + \phi\right) + u_z \end{aligned} \tag{2.18}$$

where

$$s = \frac{3J_2 R_e^2}{8a^2}\left[1 + 3\cos\left(2i_l\right)\right]$$

$$c = \sqrt{1+s}$$

J_2 (the second zonal harmonic coefficient of order 0) $= 1{,}082.6 \times 10^{-6}$

and i_l is the inclination of the leader satellite orbit and ϕ is a phase constant that depends on the initial position and velocity in the cross track plane. Assume that the inclination of the follower satellite, $i_f = i_l$, we have

$$\begin{aligned} k &= nc + \frac{3nJ_2 R_e^2}{2a^2}\left[\cos i_f\right]^2 \\ l &= 0 \end{aligned} \tag{2.19}$$

Note that if the J_2 perturbation is ignored, i.e. $s = 0$, then the modified linearized equations (2.18) reduces to the linearized HCW equations (2.16). Hence, in this report, the modified linearized HCW equations (2.16) are used in the preliminary formation controller design via MatLab and STK numerical simulation of the fully nonlinear dynamics with high fidelity force modelling including J_2-perturbation, orbital perturbation forces such as solar radiation pressure, drag will be performed on the overall designed system.

3. FORMATION DESIGN

3.1 Formation Geometry

The first part of formation control design is to determine a formation geometry to meet mission objectives and which requires reasonable propellant to maintain the formation in the presence of orbital disturbances and perturbation. Formations based on the linearized HCW homogeneous equations in (2.12) yield the following relative motion solution for unperturbed circular orbit without control input:

$$\begin{aligned}
x(t) &= \left[4x(0) + \frac{2\dot{y}(0)}{n}\right] + \frac{\dot{x}(0)}{n}\sin(nt) - \left[3x(0) + \frac{2\dot{y}(0)}{n}\right]\cos(nt) \\
y(t) &= -\left[6nx(0) + 3\dot{y}(0)\right]t + \left[y(0) - \frac{2\dot{x}(0)}{n}\right] + \left[6x(0) + \frac{4\dot{y}(0)}{n}\right]\sin(nt) + \frac{2\dot{x}(0)}{n}\cos(nt) \\
z(t) &= \frac{\dot{z}(0)}{n}\sin(nt) + z(0)\cos(nt)
\end{aligned} \tag{3.1}$$

$$\begin{aligned}
\dot{x}(t) &= \dot{x}(0)\cos(nt) + \left[3x(0)n + 2\dot{y}(0)\right]\sin(nt) \\
\dot{y}(t) &= -\left[6nx(0) + 3\dot{y}(0)\right] + \left[6x(0)n + 4\dot{y}(0)\right]\cos(nt) - 2\dot{x}(0)\sin(nt) \\
\dot{z}(t) &= \dot{z}(0)\cos(nt) - z(0)n\sin(nt)
\end{aligned} \tag{3.2}$$

There is a secular drift in the traverse, cross track component y. A bounded periodic relative motion can be obtained with the following initial conditions:

$$\dot{y}(0) = -2nx(0) \tag{3.3}$$

If the above condition is satisfied, then we can re-parametrize Eqn. (3.2) into the following magnitude-phase form:

$$\begin{aligned}
x(t) &= q_x \sin(nt + \varphi_x) \\
y(t) &= q_y + 2q_x \cos(nt + \varphi_x) \\
z(t) &= q_z \sin(nt + \varphi_z)
\end{aligned} \tag{3.4}$$

where

$$
\begin{aligned}
q_x &= \frac{\sqrt{\dot{x}^2(0)+x^2(0)n^2}}{n} \\
q_y &= y(0)-\frac{2\dot{x}(0)}{n} \\
q_z &= \frac{\sqrt{\dot{z}^2(0)+z^2(0)n^2}}{n} \\
\varphi_x &= \tan^{-1}\left(\frac{nx(0)}{\dot{x}(0)}\right) \\
\varphi_z &= \tan^{-1}\left(\frac{nz(0)}{\dot{z}(0)}\right)
\end{aligned}
\tag{3.5}
$$

The above representation parameterizes an elliptical pattern of the follower around the leader. In particular,

a) In the $x-y$ plane, the relative motion is projected into an ellipse centred at $\left(0, q_y, 0\right)$ with the semi-major axes twice that of the semi-minor axes.
b) In the $y-z$ plane, the projection is an ellipse centred at $\left(0, q_y, 0\right)$ if $\varphi_x = \varphi_z$.

In comparison, the corresponding equations of motion (2.13) for the high fidelity linearized relative motion of two satellites under the influence of the J_2 perturbation are as follows [4]:

$$
\begin{aligned}
x(t) &= x(0)\cos\left(nt\sqrt{1-s}\right)+\frac{1}{n\sqrt{1-s}}\dot{x}(0)\sin\left(nt\sqrt{1-s}\right) \\
y(t) &= -\frac{2\sqrt{1+s}}{\sqrt{1-s}}x(0)\sin\left(nt\sqrt{1-s}\right)+\frac{2\sqrt{1+s}}{n(1-s)}\dot{x}(0)\cos\left(nt\sqrt{1-s}\right)+y(0)-\frac{2\sqrt{1+s}}{n(1-s)}\dot{x}(0) \\
z(t) &= \frac{\dot{z}(0)}{k}\sin(kt)+z(0)\cos(kt)
\end{aligned}
\tag{3.6}
$$

with the following initial velocity chosen to remove the offset term in $x(t)$ and the drift term in $y(t)$

$$
x(0)+\frac{\dot{y}(0)}{2n\sqrt{1+s}}=0 \Rightarrow \dot{y}(0)=-2nx(0)\sqrt{1+s} \tag{3.7}
$$

In particular, note that the angular frequency of the J_2 perturbed circular reference orbit is now corrected as

$$
n' = n\sqrt{1-s} \tag{3.8}
$$

The relation motion dynamics under the presence of the J_2 perturbation can also be expressed in the form of Eqn. (3.4) with

$$
\begin{aligned}
x(t) &= q_x' \sin\left(n't + \varphi_x'\right) \\
y(t) &= q_y' + 2q_x' \sqrt{\frac{1+s}{1-s}} \cos\left(n't + \varphi_x'\right) \\
z(t) &= q_z' \sin\left(kt + \varphi_z'\right)
\end{aligned}
\tag{3.9}
$$

$$
\begin{aligned}
q_x' &= \sqrt{\frac{\dot{x}^2(0) + x^2(0)n^2(1-s)}{n^2(1-s)}} \\
q_y' &= y(0) - \frac{2\sqrt{1+s}}{n(1-s)}\dot{x}(0) \\
q_z' &= \frac{\sqrt{\dot{z}^2(0) + z^2(0)k^2}}{k} \\
\varphi_x' &= \tan^{-1}\left(\frac{n\sqrt{1-s}x(0)}{\dot{x}(0)}\right) \\
\varphi_z' &= \tan^{-1}\left(\frac{kz(0)}{\dot{z}(0)}\right)
\end{aligned}
\tag{3.10}
$$

Remark 3.1: The relative motion equations for the elliptical reference orbit (2.13) also exhibit the following characteristics:

a) In the $x-y$ plane, the relative motion is projected into an ellipse centred at $\left(0, q_y', 0\right)$ with the semi-major axes twice that of the semi-minor axes.
b) In the $y-z$ plane, the projection is an ellipse centred at $\left(0, q_y', 0\right)$ if $\varphi_x' = \varphi_z'$.

Remark 3.2: The elliptical reference orbit also admits a periodic solution [14] with an appropriate choice of integration constants. There will be some distortion to the unperturbed circular reference orbits due to the J_2 perturbation.

Next we shall examine 3 formation geometries which are suitable to meet our mission objectives.

3.1.1 *In-Plane Formation*

The in-plane formation in the $x-y$ plane, also known as the along-track orbit (ATO) in [15] is the simplest of all satellite formation geometry. Its primary advantages lie in its simplicity in design, deployment and control. This formation is achieved by setting all the relative position and velocity initial conditions as follows:

$$
\begin{aligned}
&x(0) = 0,\ y(0) = y_0,\ z(0) = 0, \\
&\dot{x}(0) = 0,\ \dot{y}(0) = -2nx(0) = 0,\ \dot{z}(0) = 0.
\end{aligned}
\tag{3.9}
$$

Similarly, in the presence of J_2 perturbation, it can be seen from Eqn. (3.6) that the relative motion in the $x-y$ plane is also an in-plane elliptical motion, and the ATO can be achieved by modifying the initial conditions as shown below:

$$\begin{aligned} &x(0)=0,\ y(0)=2y_0,\ z(0)=0, \\ &\dot{x}(0)=0,\ \dot{y}(0)=-2nx(0)\sqrt{1+s}=0,\ \dot{z}(0)=0. \end{aligned} \tag{3.10}$$

Fig. 3.1 In-Track Formation

3.1.2 *Cross-Track Formation*

The cross-track formation is a slight variation of the in-plane formation but with the 2 satellites lying in slightly different orbital planes separated by the right ascension of the ascending node (RAAN). In the linearized HCW equations, this formation is very similar to the in-plane formation except for a cross-track oscillation due to the difference in the RAAN. This formation is achieved by setting all the relative position and velocity to zero except for $y(0)$, i.e.

$$\begin{aligned} &x(0)=0,\ y(0)=y_0,\ z(0)=z_0, \\ &\dot{x}(0)=0,\ \dot{y}(0)=-2nx(0)=0,\ \dot{z}(0)=0. \end{aligned} \tag{3.11}$$

For ease of implementation and to minimize the propellant usage, it is more practical to specify the following initial conditions:

$$\begin{aligned} &x(0)=0,\ y(0)=y_0,\ z(0)=0, \\ &\dot{x}(0)=0,\ \dot{y}(0)=-2nx(0)=0,\ \dot{z}(0)=nz_0. \end{aligned} \tag{3.12}$$

Again, in the presence of J_2 perturbation, the initial conditions have to be modified as follows:

$$\begin{aligned} &x(0)=0,\ y(0)=y_0,\ z(0)=z_0, \\ &\dot{x}(0)=0,\ \dot{y}(0)=-2nx(0)\sqrt{1+s}=0,\ \dot{z}(0)=0. \end{aligned} \tag{3.13}$$

Alternatively, similar to Eqn. (3.12), we can also achieve the desired cross track formation with the following initial conditions:

$$x(0)=0,\ y(0)=y_0,\ z(0)=0,$$
$$\dot{x}(0)=0,\ \dot{y}(0)=-2nx(0)\sqrt{1+s},\ \dot{z}(0)=kz_0.$$

Note, however, the angular frequency of the sinusoidal motion is now modified from n in Eqn. (3.1) to $k=nc+\frac{3nJ_2R_e^2}{2a^2}\left[\cos i_f\right]^2$ in Eqn. (3.6).

Fig. 3.2 Cross-Track Formation

3.1.3 *Projected Circular Orbit*

The perhaps most interesting formation, at least for earth pointing devices, is the projected circular formation [16]. That is, the formation appears as circular under the assumption that the viewpoint is on the line connecting the centre of Earth to the centre of the relative orbit. Extensions to the case of a viewpoint above or below this line is quite straightforward. The formation is achieved from imposing the following constraint that the ellipse of relative motion is projected on to the along-track/cross-track plane into a circle given by the following relationship:

$$y^2+z^2=k^2 \tag{3.14}$$

where k is the radius of the projected circle. By using Eqns. (3.4) and (3.5), the initial conditions are as follows:

$$x(0)=(k/2)\cos\theta,\ y(0)=2\dot{x}(0)/n,\ z(0)=\pm 2x(0),$$
$$\dot{x}(0)=-(kn/2)\sin\theta,\ \dot{y}(0)=-2nx(0),\ \dot{z}(0)=\pm 2\dot{x}(0).$$

where θ is the phase angle measured counter-clockwise from the z direction in the y-z plane. It is possible to place as many satellites in a circular apparent orbit with phasing angle separating them, and also as many circular orbits with radial separation, as desired. This would cause a

”pinwheel” effect from the planetary surface as the satellites rotate about the centre of the formation.

Fig. 3.3 Projected Circular Orbit Formation

3.2 Orbital Disturbance Forces on the Formation Geometry

Consider both the unperturbed relative motion in Eqn. (3.4) and the relative motion with J_2 perturbation in Eqn. (3.9), we notice in Fig. 3.4 that the solution is periodic in both cases with the initial conditions (3.3) and (3.9) respectively. Hence, there is no secular drift in both cases when (i) circular chief orbit (2) same inclination for leader and follower orbital planes and (3) no orbital disturbance forces, e.g. solar radiation pressure and drag.

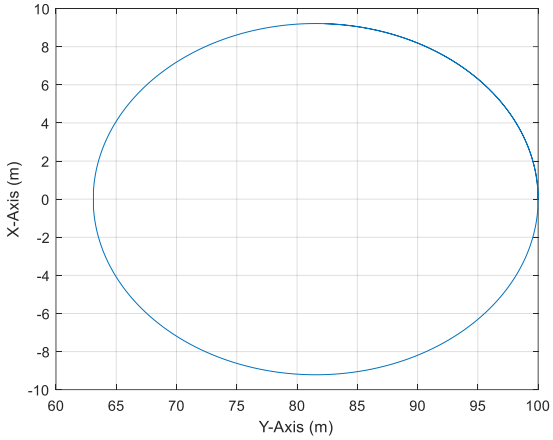

Fig. 3.4 In-Plane (x,y) Relative Motion with J_2 perturbation

Next, we consider the relative motion due to the presence of orbital disturbance forces $\begin{bmatrix} d_x & d_y & d_z \end{bmatrix}^T$ as depicted in Eqn. (2.14). The relative motion dynamics in LVLH frame is as follows:

$$\begin{aligned} \ddot{x} - 2n\dot{y} - 3n^2 x &= d_x \\ \ddot{y} \qquad\quad +2n\dot{x} &= d_y \\ \ddot{z} \qquad\quad +n^2 z &= d_z \end{aligned} \tag{3.15}$$

The disturbance is determined by environmental factors such as solar radiation pressure, air drag, etc. In the case of solar radiation pressure, there is an undamped oscillatory out of plane motion and the in-plane motion demonstrates an undamped mode at orbit rate. In [15], the exact analytical solution to Eqn. (3.15) for an inertially constant disturbance force with $\begin{bmatrix} d_x & d_y & d_z \end{bmatrix}^T$ is:

$$\begin{aligned} x &= \frac{3}{2}\frac{d_y}{n^2}\left[\sin nt - nt\cos nt\right] - \frac{d_x}{n^2}\left[\frac{3}{2}nt\sin nt - 2\left(1-\cos nt\right)\right] \\ y &= \frac{d_y}{n^2}\left[3nt\sin nt - 5\left(1-\cos nt\right)\right] + \frac{d_x}{n^2}\left[3nt - 6\sin nt + 3nt\cos nt\right] \\ z &= \frac{d_z}{n^2}\left(1-\cos nt\right) \end{aligned} \tag{3.16}$$

As is evident from the above equations, the in-plane (x,y) relative position grows without bound. Fig. 3.5 shows the uncontrolled in-plane response, obtained by numerically integrating Eq. (3.16) using a Fourier series model of the actual solar pressure forces for the relative motion solution. The actual solar pressure force magnitude and direction in inertial pace varies slightly with the orbit angle. This simulation result, shows the same behaviour as the analytic results for the spherical satellites in Eqn. (3.16), i.e., unbounded in-plane error growth over time. Clearly, this is unacceptable since the objective is to maintain the in-track position within the bounds dictated by mission requirements. Hence, some type of formation control scheme is required.

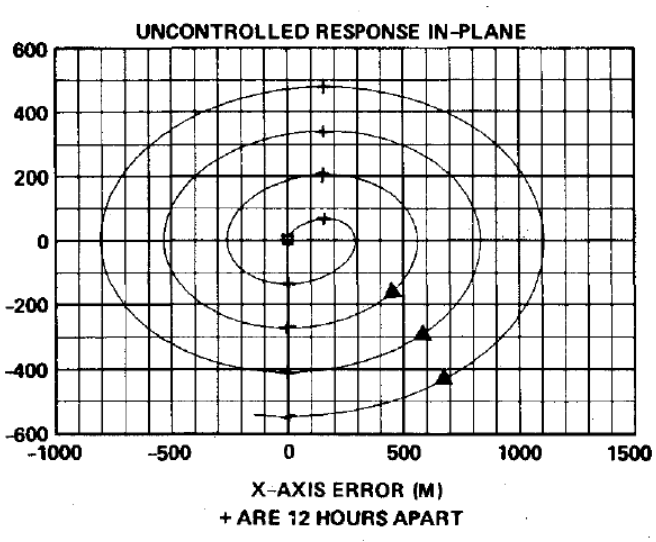

Fig. 3.5 In-Plane (x,y) Relative Motion due to Representative Solar Radiation Pressure

4. FORMATION CONTROL

The modified HCW equations describe the relative motion of a follower with respect to a leader in a reference circular orbit. They are expressed in the LVLH frame as shown in Equation (2.18). Since the modified HCW equations are a set of linear differential equations, they can be formulated in the below state space form with the state vector $\mathrm{x} = \begin{bmatrix} x & y & z & \dot{x} & \dot{y} & \dot{z} \end{bmatrix}^T$ and follower satellite control input $\mathrm{u} = \begin{bmatrix} u_x & u_y & u_z \end{bmatrix}^T$:

$$\dot{\mathrm{x}} = A\mathrm{x} + B\mathrm{u}$$

where

$$A = \begin{bmatrix} 0 & 0 & 0 & 1 & 0 & 0 \\ 0 & 0 & 0 & 0 & 1 & 0 \\ 0 & 0 & 0 & 0 & 0 & 1 \\ \left(5c^2 - 2\right)n^2 & 0 & 0 & 0 & 2nc & 0 \\ 0 & 0 & 0 & -2nc & 0 & 0 \\ 0 & 0 & -k^2 & 0 & 0 & 0 \end{bmatrix}, \; B = \begin{bmatrix} 0 & 0 & 0 \\ 0 & 0 & 0 \\ 0 & 0 & 0 \\ 1 & 0 & 0 \\ 0 & 1 & 0 \\ 0 & 0 & 1 \end{bmatrix} \tag{4.1}$$

The main goal of the formation control design is to design a controller for the follower satellite to maintain the desired formation geometry with modest control energy to fulfil mission objectives despite the presence of orbital perturbations. To minimize fuel consumption for formation keeping, [15] has proposed the use of sample-data, full-state feedback *impulsive* control scheme. Specifically, control was applied impulsively at the sampling instant based on the discrete-time model (4.1). This technique does not take into consideration the characteristics and limitations of recent developments in propulsion technologies such as chemical thrusters, Hall thrusters, pulse plasma thrusters, etc. which provide continuous thrusting over short time intervals over each orbital period. These advancements in propulsion technologies necessitate the development of *pulse-based*, spacecraft control laws. In this report, we develop pulse-based, discrete-time feedback control laws for chemical thrusters. There are two main challenges:

a. Unlike in most control problems, the application of control forces to the satellites to effect a change in the orbit can only be made over a relatively short turn on time t_{on} of 5 minutes (maximum) due to on-board satellite power and operational time limit of the chemical thrusters and also thermal considerations. The satellite motion will evolve in an uncontrolled manner in the remainder of the orbit.
b. The chemical thrusters will produce a constant thrust U_{max} of ~1N (though it will reduce as the propellant tank pressure decreases with depletion of the propellant), and thus we shall implement pulse-based thrust control via a pulse width modulation (PWM) strategy. Using the PWM strategy, the thruster turn on time t_{on} is varied while the thrust magnitude U_{max} remains almost constant.

Remark 4.1: Note that, since the in-track and cross-track motions are linearly decoupled, we can design their controllers separately. However, for ease of implementation as there is only a single thruster, we shall design both the in-track and cross-track control simultaneously.

4.1 State Feedback Controller Design

We begin by considering a periodic discrete-time feedback control system of the following form [17, 18] :

$$\mathrm{x}(k+1) = \Phi \mathrm{x}(k) + \Gamma \mathrm{u}(k), \qquad k = 0,1,..., \tag{4.2}$$

$$\mathrm{u}(k) = \begin{cases} K\mathrm{x}(k), & k = nN, \ldots, nN + p - 1 \\ 0, & k = nN + p, \ldots, nN + p + q - 1 \end{cases} \tag{4.3}$$

$n = 0,1,2,\ldots$ and $N = p + q$ is the number of samples, with sampling interval T_s, in one complete cycle over which the control is first turned on for p samples and then off for the remaining q samples and where Eqn. (4.2) is the sampled-date representation of the continuous-time, state-space model (4.1) with

$$\Phi = e^{AT_s}, \ \Gamma = \int_0^{T_s} e^{A(T_s - s)} ds B \tag{4.4}$$

$$\mathrm{x}(k) = \begin{bmatrix} x(k) & y(k) & z(k) & \dot{x}(k) & \dot{y}(k) & \dot{z}(k) \end{bmatrix}^T,$$
$$\mathrm{u}(k) = \begin{bmatrix} u_x(k) & u_y(k) & u_z(k) \end{bmatrix}^T.$$

Using a recursive procedure, we obtain the following solution for (4.2):

$$\mathrm{x}(nN) = \left[\Phi^q \left(\Phi + \Gamma K \right)^p \right]^n \mathrm{x}(0), \quad n = 1,2,\ldots \tag{4.5}$$

The stability of the closed loop system (4.2), (4.3) is ensured when the solution of Eqn. (4.5) is asymptotically stable. This is achieved by designing the control gain K, using for example Linear Quadratic Regulator (LQR) [18] or pole placement technique, such that the closed loop poles of $\Phi^q \left(\Phi + \Gamma K \right)^p$ remain within the unit disk. We shall next apply LQR state feedback control to determine the control gain K for formation keeping control. LQR control was adopted as it leads to linear control laws that are easy to design, implement and analyse with good stability margins and sensitivity properties. The LQR optimizes a quadratic cost function of states and control.

We shall consider the case where p =1 which corresponds to a single pulse over a period of $N.T_s$. This situation depicts the actual implementation constraint as the chemical thruster can only turn on over a short time with constant thrust due to thermal and electrical power constraint. The satellite motion will evolve in an uncontrolled manner in the remainder of the orbit. Hence, consider the following equivalent discrete-time auxiliary dynamic model of Eqn. (4.2) with p = 1:

$$\mathrm{z}(k+1) = \hat{\Phi}\mathrm{z}(k) + \hat{\Gamma}\mathrm{v}(k) \tag{4.6}$$

where $\hat{\Phi} = \Phi^{q+1}$ and $\hat{\Gamma} = \Phi^{q}\Gamma$. The objective function of the LQR design is defined as

$$J = \sum_{k=0}^{\infty} \mathrm{z}(k)^T Q\mathrm{z}(k) + \mathrm{v}(k)^T R\mathrm{v}(k) \tag{4.7}$$

In Eqn. (4.7), *Q* is the positive semi-definite weighting matrix of the state error, *R* is the positive definite weighting matrix of the control effort. The matrices *Q* and *R* are judiciously selected to balance the state tracking error and the control cost (propellant usage) accordingly. For the envisaged mission, *Q* and *R* are set to

$$Q = \begin{bmatrix} \alpha & 0 & 0 & 0 & 0 & 0 \\ 0 & \alpha & 0 & 0 & 0 & 0 \\ 0 & 0 & \alpha & 0 & 0 & 0 \\ 0 & 0 & 0 & 1 & 0 & 0 \\ 0 & 0 & 0 & 0 & 1 & 0 \\ 0 & 0 & 0 & 0 & 0 & 1 \end{bmatrix}, \quad R = \frac{\beta}{\alpha}\begin{bmatrix} 1 & 0 & 0 \\ 0 & 1 & 0 \\ 0 & 0 & 1 \end{bmatrix} \tag{4.8}$$

where α and β are positive tuning parameters. The optimal control law for Eqn. (4.7) is given by the linear state-feedback formula:

$$\mathrm{v}(k) = K\mathrm{z}(k) \tag{4.9}$$

where the controller gain matrix *K* is expressed as

$$K = -\left(R + \hat{\Gamma}^T P\hat{\Gamma}\right)^{-1}\hat{\Gamma}^T P\hat{\Phi} \tag{4.10}$$

and *P* is the semi-definite matrix solution of the following discrete-time Algebraic Ricatti Equation (ARE)

$$\hat{\Phi}^T P\hat{\Phi} - P + Q - \hat{\Phi}^T P\Gamma\left(R + \hat{\Gamma}^T P\hat{\Gamma}\right)^{-1}\hat{\Gamma}^T P\hat{\Phi} = 0 \tag{4.11}$$

4.2 State Feedback Control Law Implementation

Implementation of the distributed spacecraft formation flying concept requires tight, autonomous, cooperative, real-time control of the relative distance between the participating spacecraft. This will necessitate equipping all the spacecraft to interact with system-wide common capabilities (communication, sensing, navigation, control, etc.) and to operate collaboratively in a tight and real-time manner. However, for our envisaged missions, only a 'loose' satellite formation flying configuration is required. Hence, a ground-based command and control system for relative positioning of multiple spacecraft shall be implemented which sends periodic corrective control commands via uplink for formation keeping and reconfiguration. This concept of operation is illustrated in Fig 4.1.

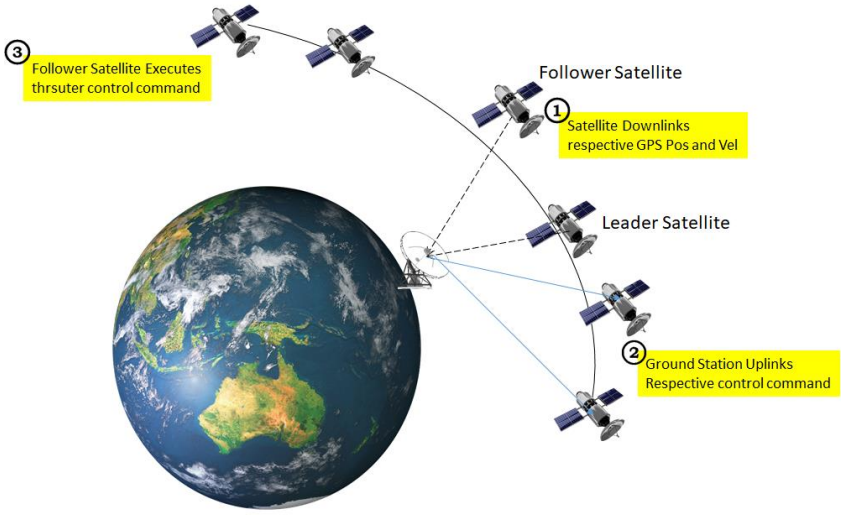

Fig. 4.1 Ground-Based Control Operation

The proposed sequence of operation is detailed in the flowchart as shown in Fig. 4.2.

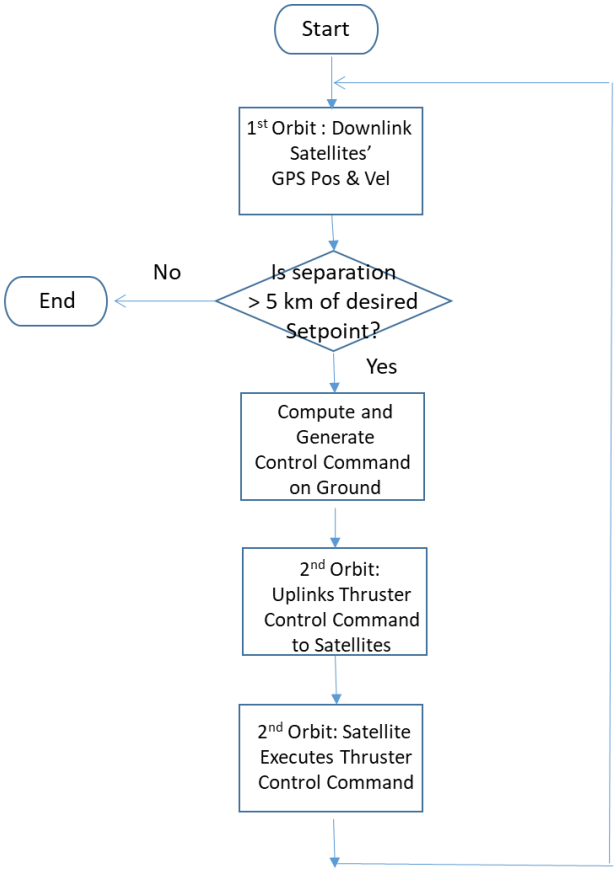

Fig. 4.2 Flowchart of Sequence of Ground-Based Control Operation

closed-loop stability cannot be rigorously guaranteed based on such a design. In recent research **[ll],** we developed a new pulse-based control scheme for DSFM which guarantees closed-loop asymptotic stability of separated spacecraft relative motion dynamics with only intermittent control action.
This methodology has been extended to non-zero set-point tracking control using a combination of feedback and feedforward control techniques.
The control input is applied for a small number of segments at the beginning of each period and it remains zero for the remaining portion of the period. However, the results of [ll] were limited to the case where control was applied for only one segment.

The control acceleration (4.3) with the gain K given in Eqn. (4.9) is used for thrusting the satellite subject to the maximum thrust per unit mass $U_{\max}$ and maximum operating time T_s in each cycle of period $N.T_s$ (which could be set to be close to 1 orbit, for instance). Since the spacecraft has only a single axis of thrust, 3 minutes in each orbital period is allotted for reorienting the thrust axis prior to the thrusting. The computed control is converted to a pulse width modulated (PWM) pulse which shall not exceed T_s. At the beginning of each cycle, the thruster on time t_{on} is computed as follows:

$$t_{\text{on}} = \frac{|u_T|}{U_{\max}} T_s \tag{4.12}$$

where

$$|u_T| = \begin{cases} |u| \quad , & \text{if } |u| \le U_{\max} \\ U_{\max} \ , & \text{otherwise} \end{cases} \tag{4.13}$$

and $|u|$ is the magnitude of the control forces computed from the state feedback law in Eqn. (4.4), $U_{\max}$ is the maximum thrust per unit mass from the thruster. Since there is only a single axis of control for the follower satellite, a unit vector in the direction of the thrust is first calculated from

$$\hat{u} = \frac{u}{|u|} \tag{4.14}$$

Since the maximum turn on time for the thrusters per orbit is limited to 5 minutes and each orbit is about 90 minutes, the following controller scheme as shown in Fig. 4.1 is implemented in each orbit.

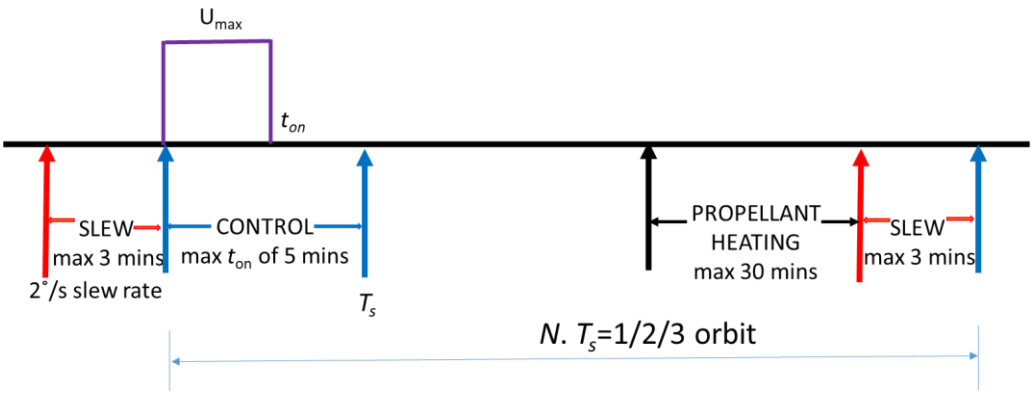

Fig. 4.1 Control Law Implementation

Thus, the generated control thrust u_i in the original continuous system (4.1) for the *i*-th orbital period is applied as follows:

$$u_i(t) = \begin{cases} U_{\max}\hat{u}_i & , \quad 0 \le t \le t_{i_{on}} = \dfrac{|u_{T_i}|}{U_{\max}} T_s \\ 0 & , \quad t_{i_{on}} < t \le N \cdot T_s \end{cases} , \tag{4.15}$$

5. MATLAB/SIMULINK SIMULATION

The designed control law (4.15) is evaluated using MatLab/Simulink for both In-Track Formation and Cross-Track Formation. The linear model system model described in Eqn. (4.1) is used without any external perturbation.

5.1 In-Track Formation

We first consider the In-Plane formation. We assume that after launch, the leader satellite is assumed to be ahead of the follower satellite and in a circular orbit at 585 km with 10 deg inclination. Initially, the follower satellite is at a position of $x_0 = [10\text{km} \quad 1000\text{km} \quad 5\text{km} \quad 10\text{m/s} \quad 20\text{m/s} \quad 50\text{m/s}]^T$. The desired in-track formation is for the follower satellite to be maintained at the position of $[0 \quad 200\text{km} \quad 0]^T$. The closed loop behaviour is simulated using the LQR feedback continuous controller and the orbital dynamics including the J_2 perturbation. A plot of the orbit trajectory in the Hill Frame is shown in Fig 4.2. The entire correction is performed using continuous firing without consideration of the $U_{\max}$ and T_s limits.

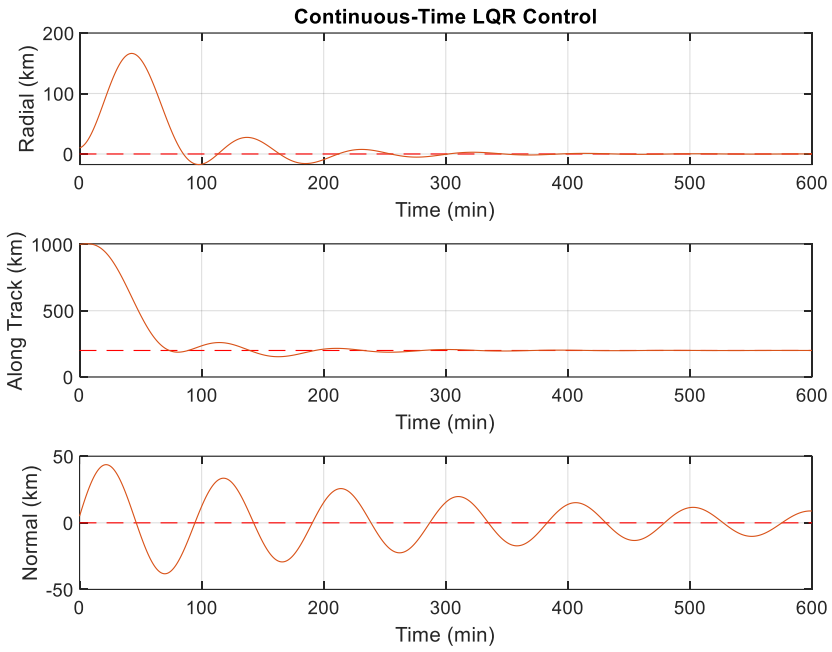

Fig. 4.2 LQR Closed-loop Follower Satellite Trajectory in Hill Frame

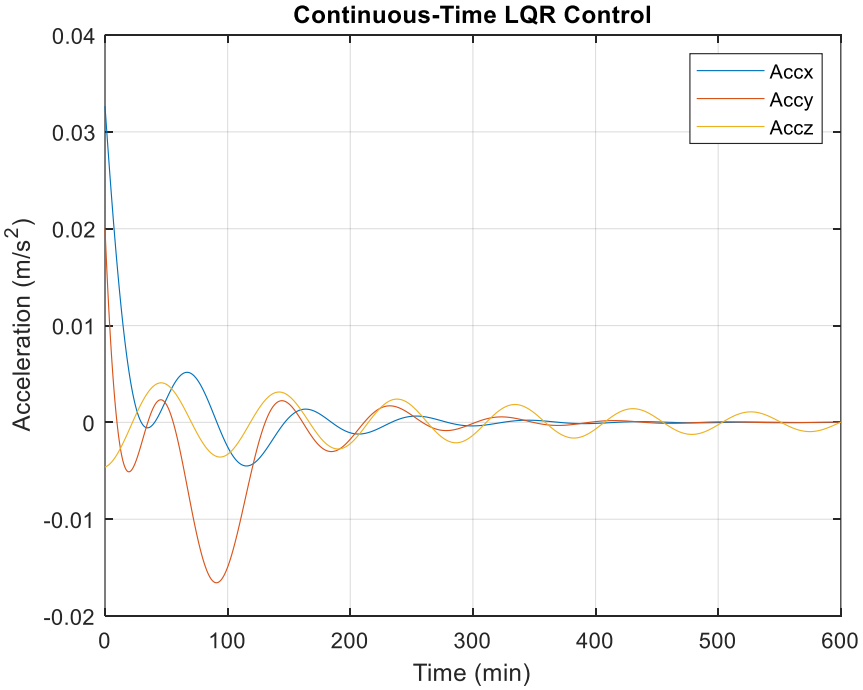

Fig. 4.3 LQR Control Acceleration

The closed loop eigenvalues are located as follows: [-0.0004 - 0.0003i, -0.0004 + 0.0003i , -0.0002 - 0.0011i, -0.0002 + 0.0011i, -0.0000 - 0.0011i, -0.0000 + 0.0011i]. Subsequently, a PWM control based on the control design in Eqns (4.7)-(4.9) was implemented and simulated using Simulink. The closed-loop results are plotted in Fig. 4.4 below.

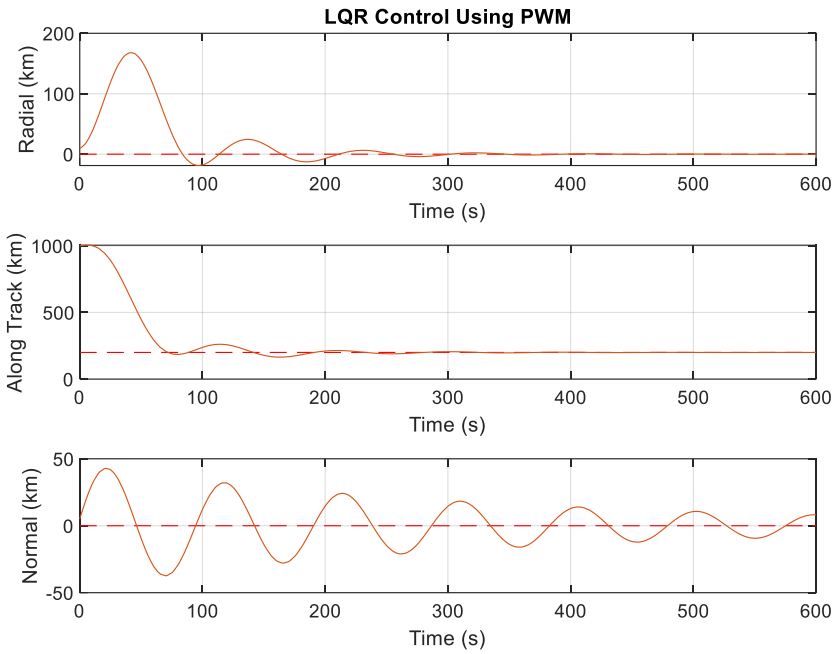

Fig. 4.4 LQR PWM Closed-loop Follower Satellite Trajectory in Hill Frame

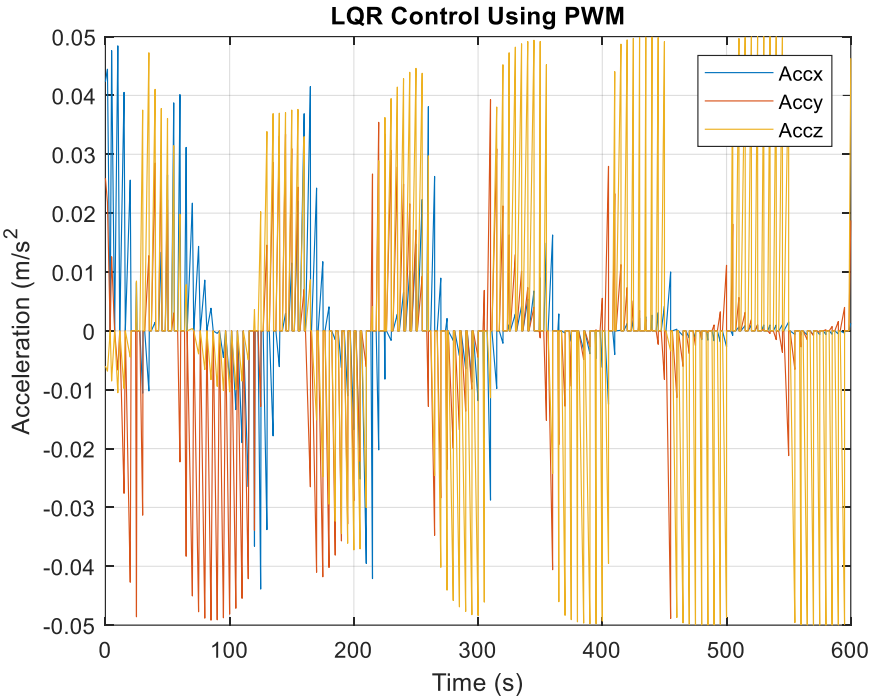

Fig. 4.5 LQR Control Acceleration

6. NON-LINEAR SIMULATION USING STK

High fidelity nonlinear simulation analysis was carried out by using the Satellite Tool Kit (STK). STK is a useful tool for simulation and visualization.

REFERENCES:

[1] Hill, G.W., "Researches in the Lunar Theory," *American Journal of Mathematics*, Vol. 1, No. 1, 1878 pp 5-26.

[2] Clohessy, W.H., and Wiltshire, R.S., "Terminal Guidance System for Satellite Rendezvous," *Journal of the Aerospace Sciences*, Vol. 27, No. 9, 1960, pp. 653-658.

[3] Vallado, D.A., *Fundamentals of Astrodynamics and Applications*, 2nd Ed. Space Technology Library, Microcosm, Segundo, CA, and Kluwer Academic , Dordrecht, The Netherlands, 2001.

[4] Schweighart, S.A., and Sedwick, R.J., "High-Fidelity Linearized J_2 Model for Satellite Formation Flight," *Journal of Guidance, Control and Dynamics*, Vol. 25, No. 6, 2002, pp. 1073-1080.

[5] Lawden, D.F., "Fundamentals of Space Navigation," *Journal of the British Interplanetary Society*, Vol. 13, No. 2, 1954, pp. 87-101.

[6] Tschauner, J., and Hempel, P., "Optimale Beschleunigungs-propgramme fur des rendezvous Manover," *Astronautica Acta*, Vol. 10, Nos. 5-6, 1964, pp. 296-307.

[7] Carter, T.E., "New Form for the Optimal Rendezvous Equations Near a Keplerian Orbit," *Journal of Guidance, Control, and Dynamics*, Vol. 13, No. 1, 1990, pp. 183-186.

[8] Lane, C., and Axelrad P., "Formation Design in Eccentric Orbits Using Linearized Equations of Relative Motion," *Journal of Guidance, Control, and Dynamics*, Vol. 29, No. 1, 2006, pp 146-160.

[9] Inalhan, G., Tillerson, M., and How, P.J., "Relative Dynamics and Control of Spacecraft Formations in Eccentric Orbits," *Journal of Guidance, Control, and Dynamics*, Vol. 25, No. 1, 2002, pp 48-59.

[10] Koenig, A., Guffanti, T., and D'Amico, S., "New State Transition matrices for Relative Motion of Spacecraft Formations in Perturbed Orbits," *AIAA/AAS Astrodynamics Specialist Conference*, AIAA SPACE Forum, Long Beach, CA, Sept, 13-16, 2016, DOI 10.2514/6.2016-5635.

[11] Brouwer, D.A., "Solution of the Problem of Artificial Satellite Theory Without Drag," *The Astronomical Journal*, Vol. 64, No. 1274, 1959, pp. 378-396.

[12] Sparks, A., "Satellite Formation Keeping in the Presence of Gravity Perturbations," Proceedings of the American Control Conference, Arlington, VA, 2001.

[13] Wang, D., Wu, B., Poh E.K., *Satellite Formation Flying – Relative Dynamics, Formation Design, Fuel Optimal Maneuvers and Formation Maintenance*, Springer, 2017.

[14] Alfriend, K.T., Vadali, S.R., Gurfil, P., How, J.P., Breger, P.S., *Spacecraft Formation Flying – Dynamics, Control and Navigation*, Elsevier Astrodynamics Series, Elsevier Ltd, Oxford, UK, 2010.

[15] Vassar, R.H., and Sherwood, R.B., "Formationkeeping for a Pair of Satellites in a Circular Orbit," AIAA Journal of Guidance, Control and Dynamics, Vol. 8, No. 2, 1985, pp. 235-242.

[16] Sabol, C., Burns, R., McLaughlin, C.A., "Satellite Formation Flying Design and Evolution," *Journal of Spacecraft and Rockets*, Vol. 38, No. 2, March-April 2001, pp. 270-278.

[17] Kapila, V., Sparks, A.G., Buffington, J.M., and Yan, Q., "Spacecraft Formation Flying: A Survey,", *Proceedings of the American Control Conference*, San Diego, CA, June 1999, pp. 4137-4141.

[18] Yan, Q., Kapila, V., Sparks, A.G., "Pulse –Based Periodic Control for Spacecraft Formation Flying,", *Proceedings of the American Control Conference*, Chicago, IL, June 2000, pp. 374-378.

[19] Bonin, G., Roth, N., Armitage, S., Newman, J., Risi, B., Zee, R.E., "CanX-4 and CanX-5 Precision Formation Flight: Mission Accomplished!," *29th Annual AIAA/USU Conference on Small Satellites*, Logan, UT, 2015.